Bifunctional Electrocatalysts

International Edition: DOI: 10.1002/anie.201503612
German Edition: DOI: 10.1002/ange.201503612

Integrating NiCo Alloys with Their Oxides as Efficient Bifunctional Cathode Catalysts for Rechargeable Zinc–Air Batteries**

Xien Liu, Minjoon Park, Min Gyu Kim, Shiva Gupta, Gang Wu, and Jaephil Cho**

Abstract: *The lack of high-efficient, low-cost, and durable bifunctional electrocatalysts that act simultaneously for the oxygen reduction reaction (ORR) and the oxygen evolution reaction (OER) is currently one of the major obstacles to commercializing the electrical rechargeability of zinc–air batteries. A nanocomposite CoO-NiO-NiCo bifunctional electrocatalyst supported by nitrogen-doped multiwall carbon nanotubes (NCNT/CoO-NiO-NiCo) exhibits excellent activity and stability for the ORR/OER in alkaline media. More importantly, real air cathodes made from the bifunctional NCNT/CoO-NiO-NiCo catalysts further demonstrated superior performance to state-of-the-art Pt/C or Pt/C + IrO_2 catalysts in primary and rechargeable zinc–air batteries.*

Highly active and durable bifunctional catalysts for the ORR and OER are essential components for developing electrically rechargeable zinc–air batteries.[1] Although Pt-, Ru-, or Ir-based materials have been widely accepted as the most active catalysts for the ORR or OER, the scarcity and high cost have limited their widespread applications in clean energy technology.[2] Recently, precious-metal-free bifunctional oxide catalysts have attracted considerable attention, including Co_3O_4 nanowire arrays,[3] perovskite $Ba_{0.5}Sr_{0.5}Co_{0.8}Fe_{0.2}O_{3-\delta}$,[4] Co_3O_4/graphene,[5] Co_xO_y/NC,[6] and spinel oxides $Co_xMn_{3-x}O_4$.[7] Some of them, such as $NiCo_2O_4$,[8] C-CoPAN900,[9] CoS_x/NS-GN,[10] and (CoO/N-CNTs + NiFe-LDH/CNT)[11] have been further implemented into real air cathodes for rechargeable zinc–air batteries. Those catalysts that solely contain oxides generally show low activity owing to their self-accumulation and insufficient electrical conductivity.[12] It was believed that combining metal oxides and conductive nanocarbon materials such as graphene and carbon nanotubes is an effective approach to enhancing catalytic activity of oxides,[5,13] through increasing number of available active sites and providing efficient charge transport channels.[14] In previous reports, nickel or cobalt oxides exhibited high intrinsic activity for either the OER or the ORR, such as CoO/NCNT,[13c] NiO,[15] and Co/CoO/graphene.[13a] Also, metallic NiCo alloys are able to provide additional synergistic properties during the electrocatalysis. Notably, the dissimilarity in lattice strain between Ni and Co creates the difference in their redox potentials and structural ordering.[16] Thus, coupling NiCo alloys with semiconductor metal oxides is highly expected to improve catalytic activity, as the formation of the Schottky barrier between NiCo alloys and metal oxides is favorable for charge separation.[17] It would be an effective strategy to design a bifunctional electrocatalyst for the ORR and OER by integrating NiCo alloys and their oxides with much improved performance.

Herein, we report a new bifunctional electrocatalyst consisting of dominant NiCo alloy coupled with a small fraction of their oxides, which are further deposited on nitrogen-doped carbon nanotubes (labeled as NCNT/CoO-NiO-NiCo). The newly developed NiCo-based catalysts is distinguished from the reported $Ni_xCo_{3-x}O_4$, $Ni_xCo_{1-x}(OH)_2$, $Ni_xCo_{2-x}O_4$, and pure NiCo alloys from the structural point of view. The bifunctional catalyst exhibits excellent activities for the ORR and the OER, along with exceptionally high performance for primary and rechargeable zinc–air batteries. In particular, the primary zinc–air battery with the cathode shows a specific capacity of 594 and 545 $mAh\,g_{zn}^{-1}$ corresponding to gravimetric energy densities of 713 and 615 $Wh\,kg_{zn}^{-1}$ when current densities are 7 and 20 $mA\,cm^{-2}$, respectively. Notably, these battery tests are carried out on only air, instead of pure O_2. Furthermore, rechargeable zinc–air battery tests indicated a high round-trip efficiency evidenced by a narrow discharge–charge voltage gap and stable voltage plateau during charging–discharging up to 100 cycles at a current density of 20 $mA\,cm^{-2}$.

An optimized mol ratio of $Ni(NO_3)_2{\cdot}6H_2O$ and $Co(NO_3)_2{\cdot}6H_2O$ (Ni/Co = 1:1) was reacted with mildly oxidized CNT at 150 °C in urea solution by a simple hydrothermal procedure in a 50 mL autoclave. The resultant precursor CNT/$Ni_{1-x}Co_x(OH)_2$ was finally transformed to NCNT/CoO-NiO-NiCo nanocomposite through a thermal annealing step at 500 °C in a NH_3/Ar atmosphere. The identical procedures were carried out for the preparation of monometallic Co- and Ni-based catalysts (NCNT/CoO-Co and NCNT/NiO-Ni; for

[*] Dr. X. Liu, M. Park, Prof. J. Cho
Department of Energy Engineering
School of Energy and Chemical Engineering
National Institute of Science and Technology (UNIST)
Ulsan 689-798 (Korea)
E-mail: jpcho@unist.ac.kr
Dr. M. G. Kim
Beamline Research Division, Pohang Accelerator Laboratory (PAL)
Pohang 790-784 (Korea)
S. Gupta, Prof. G. Wu
Department of Chemical and Biological Engineering
University at Buffalo, State University of New York
Buffalo, NY 14260 (USA)
E-mail: gangwu@buffalo.edu

[**] This work was supported by the next generation secondary battery R&D program of MKE/KEIT (10042575). The authors wish to acknowledge the Pohang Light Sources (PLS) for XAS measurements. G.W. is also grateful the financial support from the startup fund of University at Buffalo, SUNY along with U.S. Department of Energy, Fuel Cell Technologies Office (FCTO) Incubator Program (DE-EE0006960).

Supporting information for this article is available on the WWW under http://dx.doi.org/10.1002/anie.201503612.

details, see the Supporting Information). According to SEM and TEM images (Figure 1 a–c), CoO-NiO-NiCo composite nanoparticles are clearly supported on the CNTs. The lattice fringes with *d*-spacing values of 2.12 Å and 2.06 Å correspond to the (200) and (111) crystal planes for CoO (or NiO) and Co (or Ni), respectively. The elemental composition was analyzed by using HAADF-STEM-EDS (Supporting Information, Figure S1), which shows that the content of O is significantly lower than those of Co and Ni. The atomic ratio of Co and Ni was determined to be 52/48 by using inductively coupled plasma optical emission spectroscopy (ICP-OES), which is in good agreement with the result from EDS. The monometallic NCNT/CoO-Co and NCNT/NiO-Ni were also fully characterized by using HRTEM, XRD, and HAADF-STEM (Supporting Information, Figures S2–S5). The XRD patterns of precursor, monometallic, and NiCo alloyed-based catalysts in Figure 1 d reveal that the dominant phases of nanocomposites are metallic alloy structures showing diffraction peaks at 44.4°, 51.7°, and 76.1° that can be assigned to the (111), (200), and (220) crystal planes, respectively, for metallic Ni (JCPDS 04-0850), Co (JCPDS 15-0806), and Ni-Co alloy.[18] The XRD pattern of NCNT/CoO-NiO-NiCo is significantly different from reported $Ni_{1-x}Co_xO$, $Ni_xCo_{2-x}O_4$, $Ni_xCo_{3-x}O_4$, and $Ni_{1-x}Co_xO_y$,[19] indicating an intrinsically different structure (see XRD results of precursor, NCNT/CoO-Co and NCNT/NiO-Ni in the Supporting Information, Figures S2 and S4). The surface composition of catalysts are further examined by XPS and XANES, which further provide insight into the structure of NCNT/CoO-NiO-NiCo The full XPS spectra of CNT/$Ni_{1-x}Co_x(OH)_2$ and NCNT/CoO-NiO-NiCo are recorded in the Supporting Information, Figure S6 a. All elements including C, O, N, Ni, and Co were detected. The percentages of element N are approximately 2.65 at% and 3.54 at% for CNT/$Ni_{1-x}Co_x(OH)_2$ and NCNT/CoO-NiO-NiCo, respectively. The formation of NiO and CoO also was confirmed by comparing the high resolution O 1s spectra of CNT/$Ni_{1-x}Co_x(OH)_2$ and NCNT/CoO-NiO-NiCo (Supporting Information, Figure S6 b,c), in which the peak of 529.7 eV is a typical the presence of lattice oxide oxygen from CoO or NiO. For XANES (Figure S9 a,c), the Co and Ni K edge in the principal absorption peaks are at about 7725 and 8351 eV, accompanying metallic Co and Ni species at circa 7712 and 8336 eV, respectively. For EXAFS, the strongest peak is shifted to lower interatomic distance for NCNT/CoO-NiO-NiCo (ca. 2.16 Å), compared to Co foil (ca. 2.18 Å), indicative of increased content of CoO in the surface layers of catalysts (Supporting Information, Figure S9b). The strongest peak is assigned to Co–Co interactions from metallic Co part. There is no fine structure of peaks and valleys observed at the range of 3.0 to 5.0 Å, instead of a broad peak, which is different from NCNT/CoO-Co, indicating a distinct local neighbor environment of Co atoms. This is attributed to strong hybridization of Ni and Co. Likewise, similar broad peak is observed at the range of 3.0 to 5.0 Å for Ni K-edge EXAFS spectra (Supporting Information, Figures S9 d and S10d).

During the OER activity measurement, the NCNT/CoO-NiO-NiCo shows a significantly low overpotential (ca. 0.27 V) compared to NCNT/NiO-Ni (0.40 V), NCNT/CoO-Co (0.38 V), and state-of-the-art IrO_2 (0.39 V) at a current density of 10 mA cm^{-2} (Figure 2 a). Also, NCNT/CoO-NiO-NiCo exhibited a much lower Tafel slope (40 mV dec^{-1}) relative to NCNT/CoO-Co (64 mV dec^{-1}), NCNT/NiO-Ni (80 mV dec^{-1}), and IrO_2 (65 mV dec^{-1}) (Figure 2 b). A lower Tafel slope usually suggests higher OER activity. The overpotential of the OER on NCNT/CoO-NiO-NiCo catalyst is decreased by 110 and 130 mV compared to those of NCNT/CoO-Co and NCNT/NiO-Ni, respectively (Figure 2 c). Also, the current density of NCNT/CoO-NiO-NiCo measured at $\eta = 300$ mV is increased by 6.2- and 8.3-fold compared to

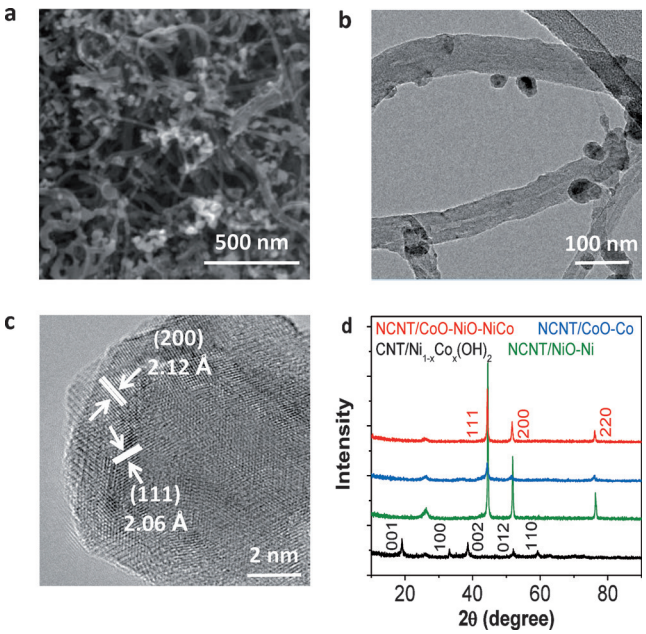

Figure 1. a) SEM image of NCNT/CoO-NiO-NiCo. b),c) HRTEM images of NCNT/CoO-NiO-NiCo. d) XRD spectra of CNT/$Ni_{1-x}Co_x(OH)_2$, NCNT/NiO-Ni, NCNT/CoO-Co, and NCNT/CoO-NiO-NiCo.

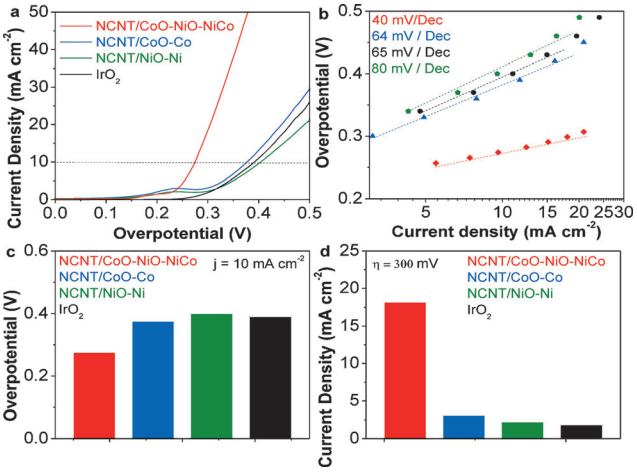

Figure 2. Electrochemical OER catalytic activity of NCNT/NiO-Ni, NCNT/CoO-Co, NCNT/CoO-NiO-NiCo, and IrO_2. a) OER polarization curves (the loading of sample was 0.21 mg cm^{-2} at the scanning rate of 10 mV s^{-1} in 1.0 M KOH solution). b) Tafel plots derived from OER polarization curves. c) Overpotentials needed to achieve the current density of 10 mA cm^{-2}. d) Current densities at $\eta = 300$ mV.

monometallic NCNT/CoO-Co and NCNT/NiO-Ni, respectively (Figure 2d). Of note, the activity of NCNT/CoO-NiO-NiCo significantly outperforms IrO_2 nanoparticles, and even NCNT/CoO-Co and NCNT/NiO-Ni perform comparably to IrO_2. We also compare our catalysts with some other reported precious-metal-free oxide electrocatalysts. In particular, during the OER, the NCNT/CoO-NiO-NiCo is able to generate a current density of 19 mA cm^{-2} at an overpotential of 0.3 V, which is obviously higher than those measured with the catalysts listed in the Supporting Information, Table S3. It is worth noting that the remarkable activity measured with the NCNT/CoO-NiO-NiCo catalyst is mainly contributed from CoO-NiO-NiCo, owing to the fact that the NCNT alone showed a very poor activity for the OER (Supporting Information, Figure S12a).

Furthermore, during the ORR studies, the NCNT/CoO-NiO-NiCo catalyst exhibits an onset potential of 0.97 V and a half-wave potential of 0.83 V (vs. RHE) that is more positive relative to NCNT/NiO-Ni (0.75 V) and NCNT/CoO-Co (0.80 V) samples (Figure 3a). An enhancement of activity on NCNT/CoO-NiO-NiCo is indicated by its smaller Tafel slope (63 mV dec^{-1}) relative to NCNT/NiO-Ni and NCNT/CoO-Co (100 and 73 mV dec^{-1}) (Figure 3b). Although $E_{1/2}$ of NCNT/CoO-NiO-NiCo is still more negative by 40 mV compared to Pt/C (0.87 V), its ORR activity is comparable to those of nonprecious metal-based oxide catalysts reported before (Supporting Information, Table S4). We also performed rotating ring-disk electrode (RRDE) tests to determine the electron transfer number and percentage of peroxide species using the established K-L equations (Figure 3c,d; Supporting Information, Figure S11b).[20] The average electron transfer number is 3.85 at the potential range from 0.3 to 0.8 V for NCNT/CoO-NiO-NiCo that is consistent with the peroxide yield results determined by RDE (Supporting Information, Figure S11a). The average electron-transfer numbers are approximately 3.25 and 3.45 for NCNT/NiO-Ni and NCNT/CoO-Co, respectively. The percentage of peroxide yield relative to the total reduction products for NCNT/CoO-NiO-NiCo is about 10%, which is significantly lower than NCNT/NiO-Ni (ca. 40%) and NCNT/CoO-Co (ca. 25%). Thus, NCNT/CoO-NiO-NiCo catalysts is capable of reducing O_2 through a highly desirable four-electron to OH^- in alkaline media, rather than two-electron to peroxide. Compared to the NCNT/CoO-NiO-NiCo catalyst, NCNT alone also shows a lower ORR activity (Supporting Information, Figure S12b), indicating the insignificant contribution of NCNT to the overall high activity. We also tested the ORR polarization curves of NCNT/NiO-Ni, NCNT/CoO-Co, and NCNT/CoO-NiO-NiCo with other two different Ni-to-Co ratios (Ni/Co = 2:1 or 1:2 in the starting materials; Supporting Information, Figure S13). They all exhibited poor electrocatalytic performance compared to the best-performing NCNT/CoO-NiO-NiCo (Ni/Co = 1:1 in the starting materials). We also tested ORR polarization curves of NCNT/CoO-Co, NCNT/NiO-Ni, and NCNT/CoO-NiO-NiCo in 0.1 M KOH with the loading of 0.21 mg cm^{-2} (Supporting Information, Figure S14), in which the ORR performance of catalysts are similar to those measured in 1 M KOH solution. Furthermore, the NCNT/CoO-NiO-NiCo catalysts show excellent stability during the OER and the ORR (Supporting Information, Figure S15). Ion and charge transports are crucial factors for efficient electrocatalysts. Thus, we measured the electrochemical impedance spectroscopy (EIS) under ORR reaction conditions (Supporting Information, Figure S16). The resistance shown in the high-frequency region is related to the uncompensated solution resistance (R_s, ohmic resistance). The charge-transfer resistances were simulated by fitting the spectra using the equivalent circuit. The NCNT/CoO-NiO-NiCo showed much less charge-transfer resistance (R_{ct}; ca. 300 Ω) compared to those of NCNT/CoO-Co (ca. 600 Ω) and NCNT/NiO-Ni (ca. 1100 Ω), indicating a fast charge-transfer rate and suggesting a synergistic effect of the Ni and Co during the ORR.

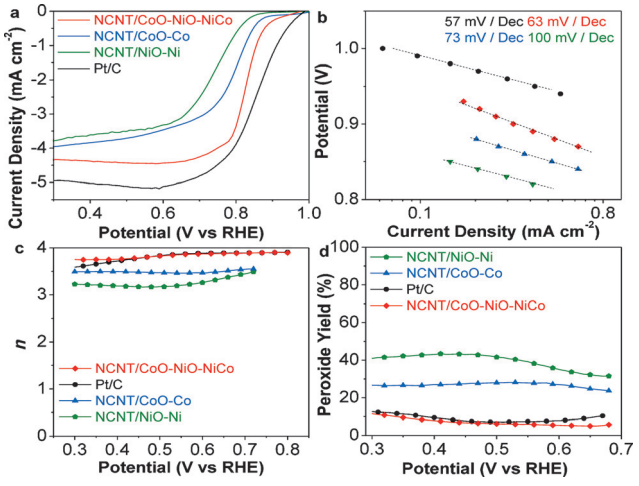

Figure 3. a) ORR polarization curves of NCNT/CoO-NiO-NiCo, reference catalysts, and Pt/C (Scanning rate: 10 mV s^{-1}, rotating rate: 1600 rpm, the loading is 0.21 mg cm^{-2}). b) The Tafel plots of NCNT/CoO-NiO-NiCo, reference catalysts, and Pt/C. c) The electron transfer number *n* of NCNT/CoO-NiO-NiCo, reference catalysts, and Pt/C at different potentials. d) Percentage of peroxide with respect to the total oxygen reduction products.

Apart from traditional electrochemical studies in aqueous electrolytes, a newly designed zinc–air cell was used to further determine the bifunctional cathode catalyst performance under real battery operation conditions. A digital photograph of the zinc–air battery is shown in the Supporting Information, Figure S17 in which an air cathode was prepared by coating a mixture of the activated charcoal and PTFE (weight ratio 7:3) on the nickel mesh, followed by the loading of NCNT/CoO-NiO-NiCo, NCNT/CoO-Co, NCNT/NiO-Ni, or Pt/C (0.53 mg cm^{-2}) on the surface of electrode. Such a fabricated cathode is separated by a nylon polymer membrane with a zinc metal anode. Nickel meshes were used as the current collectors for both electrodes. An amount of 2.0 mL 6.0 M KOH electrolyte was filled between the cathode and anode. Notably, 6.0 M KOH electrolyte is generally employed in zinc–air batteries because of its high ionic conductivity. The discharge polarization curves of our catalysts and Pt/C clearly reveal that the battery performance with NCNT/CoO-NiO-NiCo cathode is superior to those with NCNT/CoO-Co and NCNT/NiO-Ni cathodes, which is comparable to the Pt/C-based cathode (Figure 4b). The galvano-

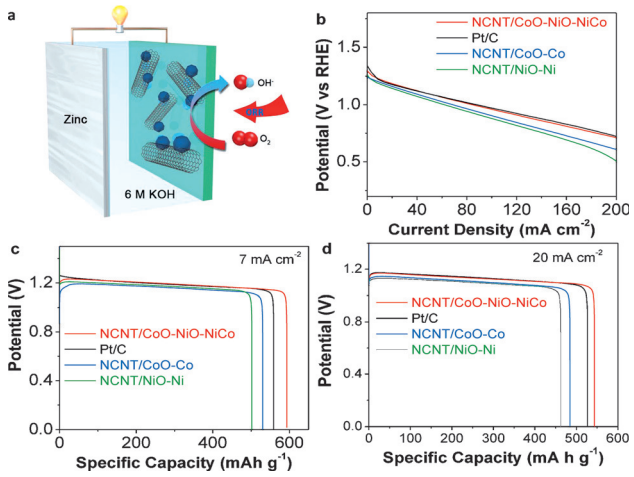

Figure 4. Electrochemical performance of the primary zinc–air batteries using NCNT/CoO-NiO-NiCo, NCNT/CoO-Co, NCNT/NiO-Ni, and Pt/C as cathode ORR catalysts in 6 M KOH. a) Illustration of the primary zinc–air batteries. b) The discharge polarization curves of NCNT/CoO-NiO-NiCo, NCNT/CoO-Co, NCNT/NiO-Ni, and Pt/C. c), d) Specific capacities of the primary zinc–air batteries normalized to the mass of the consumed Zn at the current density of 7 and 20 mA cm^{-2} (mass loading of 0.53 mg cm^{-2}).

static discharge curves in the Supporting Information, Figure S18 clearly reveal that the performance of NCNT/CoO-NiO-NiCo-based battery is superior to NCNT/CoO-Co and NCNT/NiO-Ni-based batteries at both a low and a high current density. NiCo alloy-based battery shows higher voltage plateau (ca. 1.22 and 1.08 V) at the current density of 7 and 35 mA cm^{-2}, which are comparable to the Pt/C-based battery and significantly higher than monometallic-based batteries (1.17 and 1.03 V). Only a slight potential drop is observed for each sample after a long-term galvanostatic discharge, indicating a good catalytic stability for the ORR. Figure 4c,d show that the NCNT/CoO-NiO-NiCo cathode yields the highest specific capacity relative to NCNT/CoO-Co, NCNT/NiO-Ni, and Pt/C cathodes. When normalized to the mass of consumed Zn, the battery using the NCNT/CoO-NiO-NiCo cathode exhibited the specific capacities 594 and 545 mAh g_{zn}^{-1} at current densities of 7 and 20 mA cm^{-2}, respectively. They correspond to gravimetric energy densities of 713 and 615 Wh kg_{zn}^{-1}. Conversely, the NCNT/NiO-Ni cathode showed the lowest specific capacities (502 and 463 mAh g_{zn}^{-1}) and gravimetric energy densities (582 and 504 Wh kg_{zn}^{-1}) for both current densities. We also tested the battery performance at a higher current density of 35 mA cm^{-2} (Supporting Information, Figure S19), which showed the same trends in terms of specific capacity and energy densities. Thus, the best-performing cathode in primary zinc–air batteries is the NCNT/CoO-NiO-NiCo catalyst. Furthermore, the discharge capacity of the activated charcoal air cathode without NCNT/CoO-NiO-NiCo catalyst was studied for comparison (Supporting Information, Figure S20). A dramatic drop of discharge potential and much shorter discharge time were measured with the cathode without catalyst. This comparison indicates that activated charcoal itself shows insignificant activity towards the ORR during the battery discharge.

We further investigated rechargeable zinc–air batteries using the identical configuration except for adding the zinc oxide (0.2 M) into 6 M KOH electrolyte (Figure 5a). In the case of the NCNT/CoO-NiO-NiCo cathode, the sum of charging and discharging overpotentials is 1.20 V at a current density of 50 mA cm^{-2} (Figure 5b). This value is significantly lower than those measured with NCNT/CoO-Co (1.50 V), NCNT/NiO-Ni (1.75 V), and comparable to the precious metal cathode (Pt/C + IrO_2). Notably, during long-term charge–discharge cycling tests using a constant current density of 20 mA cm^{-2}, the NCNT/CoO-NiO-NiCo cathode in rechargeable zinc–air batteries shows the highest round-trip efficiency (negligible voltage change at the end) and the smallest sum of overpotential (0.86 V) when compared with NCNT/CoO-Co and NCNT/NiO-Ni cathodes (Figure 5c). This exceptional battery performance is as good as the most active precious metal bifunctional cathode (Pt/C + IrO_2). When compared the NCNT/CoO-NiO-NiCo catalyst to all of other studied precious-metal-free oxide catalysts (Supporting Information, Table S5), it is one of the best performing bifunctional catalysts with substantially improved stability and minimized overpotentials during the discharging and charging processes. Discharge–charge cycling of two-electrode rechargeable zinc–air batteries for each samples is shown in the Supporting Information, Figure S20. Notably, we used ambient air, instead of pure O_2, which is more relevant to practical applications. Importantly, only small amount of electrolyte (2 mL 6.0 M KOH) is required to fill the space between anode and cathode in our novel zinc–air cell configuration, which is capable of generating substantial current density (Supporting Information, Figure S16). Conversely, 30–40 mL 6.0 M KOH electrolyte and pure O_2 were used for measurements of a battery by using the CoO/NCNT cathode reported

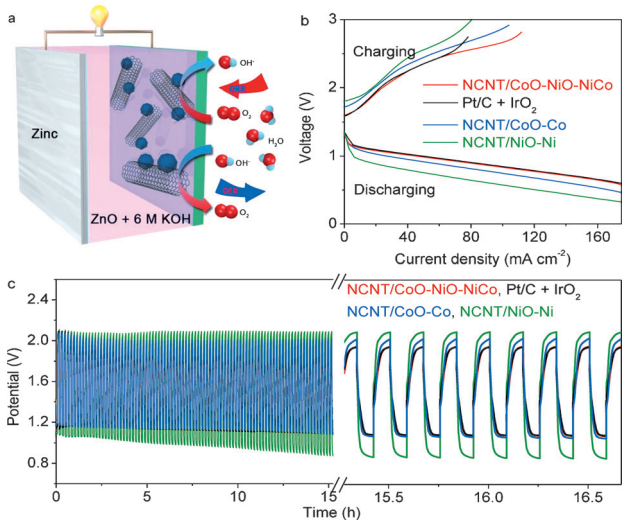

Figure 5. Electrochemical performance of the rechargeable zinc–air batteries using NCNT/CoO-NiO-NiCo, NCNT/CoO-Co, NCNT/NiO-Ni, and Pt/C as cathode ORR catalysts in 6 M KOH. a) Illustration of the rechargeable zinc–air battery. b) Charge and discharge polarization curves of two-electrode rechargeable zinc–air batteries. c) Discharge/charge cycling curves of two-electrode rechargeable zinc–air batteries at the current density of 20 mA cm^{-2}.

before.[11] Unlike our bifunctional catalyst that is simultaneously active for the ORR and the OER, an ORR-active CoO/NCNT (1.0 mg cm^{-2}) combining with an OER-active NiFe LDH/CNT (5.0 mg cm^{-2}) were used to fabricate air cathode for measuring a rechargeable zinc–air battery.[11] The loading of NCNT/CoO-NiO-NiCo used in this work is only 0.53 mg cm^{-2}, which is much lower than that of (CoO/CNT + NiFe LDH/CNT) system. In general, a low loading results in a thin cathode layer with facile mass transfer for high-power and high-rate batteries. The NCNT/CoO-NiO-NiCo is more advanced bifunctional cathode catalyst for both primary and rechargeable zinc–air batteries.

In conclusion, we reported a novel approach to preparing an effective ORR/OER bifunctional electrocatalyst for rechargeable zinc–air batteries. The highly active CoO, NiO, and NiCo alloy were synergistically integrated into a nanocomposite, followed by depositing onto an electrical conductive nanocarbon (nitrogen-doped CNTs). The resulting hybrid exhibited excellent performance as a bifunctional electrocatalyst for the ORR and the OER in a rechargeable zinc–air battery, evidenced by ever-reported discharge voltage plateau (1.22 V), high energy densities (713 and 615 Wh kg$_{zn}^{-1}$ at the current densities of 7 and 20 mA cm^{-2}, respectively) under ambient air, high round-trip efficiency, and remarkable stability up to 100 cycles at a current density of 20 mA cm^{-2}. These performance metrics measured with the NCNT/CoO-NiO-NiCo catalyst are significantly superior to the monometallic Co- and Ni-based catalysts owing to the very likely synergistic effect between Co and Ni. More importantly, the precious-metal-free bifunctional catalyst demonstrated superior or comparable performance relative to state-of-the-art precious metals, Pt/C, or (Pt/C + IrO_2)-based catalysts. This work will open a new avenue to design advanced oxide nanocomposite bifunctional catalysts as a replacement of precious metals for reversible electrochemical energy storage and conversion technologies such as metal–air batteries and fuel cells.

Keywords: bifunctional electrocatalysts · nickel–cobalt alloy · oxygen evolution reaction · oxygen reduction reaction · zinc–air batteries

How to cite: *Angew. Chem. Int. Ed.* **2015**, *54*, 9654–9658
Angew. Chem. **2015**, *127*, 9790–9794

[1] D. Sun, Y. Shen, W. Zhang, L. Yu, Z. Yi, W. Yin, D. Wang, Y. Huang, J. Wang, J. B. Goodenough, *J. Am. Chem. Soc.* **2014**, *136*, 8941–8946.
[2] N. Kakati, J. Maiti, S. H. Lee, S. H. Jee, B. Viswanathan, Y. S. Yoon, *Chem. Rev.* **2014**, *114*, 12397–12429.
[3] D. U. Lee, J. Y. Choi, K. Feng, H. W. Park, Z. W. Chen, *Adv. Energy Mater.* **2014**, *4*, 1301089.
[4] a) T. Takeguchi, T. Yamanaka, H. Takahashi, H. Watanabe, T. Kuroki, H. Nakanishi, Y. Orikasa, Y. Uchimoto, H. Takano, N. Ohguri, M. Matsuda, T. Murota, K. Uosaki, W. Ueda, *J. Am. Chem. Soc.* **2013**, *135*, 11125–11130; b) M. Risch, K. A. Stoerzinger, S. Maruyama, W. T. Hong, I. Takeuchi, Y. Shao-Horn, *J. Am. Chem. Soc.* **2014**, *136*, 5229–5232; c) J. I. Jung, H. Y. Jeong, J. S. Lee, M. G. Kim, J. Cho, *Angew. Chem. Int. Ed.* **2014**, *53*, 4582–4586; *Angew. Chem.* **2014**, *126*, 4670–4674; d) J. I. Jung, H. Y. Jeong, M. G. Kim, G. Nam, J. Park, J. Cho, *Adv. Mater.* **2015**, *27*, 266–271; e) C. F. Chen, G. King, R. M. Dickerson, P. A. Papin,, S. Gupta, W. Kellogg, G. Wu, *Nano Energy* **2015**, *13*, 423–432.
[5] Y. Y. Liang, Y. G. Li, H. L. Wang, J. G. Zhou, J. Wang, T. Regier, H. J. Dai, *Nat. Mater.* **2011**, *10*, 780–786.
[6] J. Masa, W. Xia, I. Sinev, A. Q. Zhao, Z. Y. Sun, S. Grutzke, P. Weide, M. Muhler, W. Schuhmann, *Angew. Chem. Int. Ed.* **2014**, *53*, 8508–8512; *Angew. Chem.* **2014**, *126*, 8648–8652.
[7] a) F. Y. Cheng, J. A. Shen, B. Peng, Y. D. Pan, Z. L. Tao, J. Chen, *Nat. Chem.* **2011**, *3*, 79–84; b) A. Q. Zhao, J. Masa, W. Xia, A. Maljusch, M. G. Willinger, G. Clavel, K. P. Xie, R. Schlogl, W. Schuhmann, M. Muhlert, *J. Am. Chem. Soc.* **2014**, *136*, 7551–7554.
[8] M. Prabu, K. Ketpang, S. Shanmugam, *Nanoscale* **2014**, *6*, 3173–3181.
[9] B. Li, X. M. Ge, F. W. T. Goh, T. S. A. Hor, D. S. Geng, G. J. Du, Z. L. Liu, J. Zhang, X. G. Liu, Y. Zong, *Nanoscale* **2015**, *7*, 1830–1838.
[10] D. S. Geng, N. N. Ding, T. S. A. Hor, S. W. Chien, Z. L. Liu, Y. Zong, *RSC Adv.* **2015**, *5*, 7280–7284.
[11] Y. G. Li, M. Gong, Y. Y. Liang, J. Feng, J. E. Kim, H. L. Wang, G. S. Hong, B. Zhang, H. J. Dai, *Nat. Commun.* **2013**, *4*, 1805.
[12] a) A. J. Esswein, M. J. McMurdo, P. N. Ross, A. T. Bell, T. D. Tilley, *J. Phys. Chem. C* **2009**, *113*, 15068–15072; b) J. A. Koza, Z. He, A. S. Miller, J. A. Switzer, *Chem. Mater.* **2012**, *24*, 3567–3573.
[13] a) S. J. Guo, S. Zhang, L. H. Wu, S. H. Sun, *Angew. Chem. Int. Ed.* **2012**, *51*, 11770–11773; *Angew. Chem.* **2012**, *124*, 11940–11943; b) S. Mao, Z. H. Wen, T. Z. Huang, Y. Hou, J. H. Chen, *Energy Environ. Sci.* **2014**, *7*, 609–616; c) Y. Y. Liang, H. L. Wang, P. Diao, W. Chang, G. S. Hong, Y. G. Li, M. Gong, L. M. Xie, J. G. Zhou, J. Wang, T. Z. Regier, F. Wei, H. J. Dai, *J. Am. Chem. Soc.* **2012**, *134*, 15849–15857.
[14] a) Y. Wang, H. J. Zhang, L. Lu, L. P. Stubbs, C. C. Wong, J. Y. Lin, *ACS Nano* **2010**, *4*, 4753–4761; b) T. Y. Ma, S. Dai, M. Jaroniec, S. Z. Qiao, *J. Am. Chem. Soc.* **2014**, *136*, 13925–13931.
[15] K. Fominykh, J. M. Feckl, J. Sicklinger, M. Doblinger, S. Bocklein, J. Ziegler, L. Peter, J. Rathousky, E. W. Scheidt, T. Bein, D. Fattakhova-Rohlfing, *Adv. Funct. Mater.* **2014**, *24*, 3123–3129.
[16] B. N. Wanjala, B. Fang, R. Loukrakpam, Y. S. Chen, M. Engelhard, J. Luo, J. Yin, L. F. Yang, S. Y. Shan, C. J. Zhong, *ACS Catal.* **2012**, *2*, 795–806.
[17] S. Q. Zhou, M. Wen, N. Wang, Q. S. Wu, Q. N. Wu, L. Y. Cheng, *J. Mater. Chem.* **2012**, *22*, 16858–16864.
[18] Syukri, T. Ban, Y. Ohya, Y. Takahashi, *Mater. Chem. Phys.* **2003**, *78*, 645–649.
[19] a) G. M. Kumar, D. H. Kim, J. Park, *CrystEngComm* **2013**, *15*, 8195–8201; b) F. C. Zheng, D. Q. Zhu, Q. W. Chen, *ACS Appl. Mater. Interfaces* **2014**, *6*, 9256–9264; c) X. Z. Yuan, W. Qu, X. G. Zhang, P. Yao, J. Fahlman, *ESC Transactions* **2013**, *45*, 105–112; d) L. Trotochaud, J. K. Ranney, K. N. Williams, S. W. Boettcher, *J. Am. Chem. Soc.* **2012**, *134*, 17253–17261.
[20] R. Cao, R. Thapa, H. Kim, X. Xu, M. G. Kim, Q. Li, N. Park, M. L. Liu, J. Cho, *Nat. Commun.* **2013**, *4*, 2076.

Received: April 20, 2015
Revised: June 9, 2015
Published online: June 26, 2015

